Mechanics & Industry **23**, 19 (2022)

https://doi.org/10.1051/meca/2022019

Mechanics & Industry

Available online at:
www.mechanics-industry.org

REGULAR ARTICLE

OPEN ACCESS

Study on contact load and preload characteristics of cylindrical roller bearings with triple-lobe raceway

Qing Jie Yu*, Jie Chi, Ping Gong, Hong Wei Jiang, Li Wei Zhan, and Lin Lin Xue

AECC Harbin Bearing Co., Ltd., Harbin 150025, China

Received: 8 March 2022 / Accepted: 13 June 2022

Abstract. The suitable preload design of cylindrical roller bearing with triple-lobe raceway can avoid effectively bearing sliding damage. To realize the preload characteristics analysis of bearing, the quasi-static numerical model of cylindrical roller bearing with triple-lobe raceway is established and solved by the improved Newton-Raphson method. Taking a cylindrical roller bearing with triple-lobe raceway as an example, the effects of mounting radial clearance, outer raceway waveform value, radial load and rotational speed on maximum contact load and preload of the bearing are analyzed. The results show that the preload of cylindrical roller bearing with triple-lobe raceway can be controlled by adjusting the mounting radial clearance and outer triple-lobe raceway waveform value according to the radial load and rotational speed conditions. The bearing temperature trend predicted by the preload characteristic is verified by the test. It indicates the numerical model can effectively guide the preload quantitative design of cylindrical roller bearing with triple-lobe raceway.

Keywords: Preload characteristics / triple-lobe raceway / improved Newton-Raphson method bearing temperature trend / preload quantitative design

1 Introduction

Cylindrical roller bearing mainly plays the role of rotation and support in the engine [1]. The cylindrical roller bearing with circular raceway has a greater risk of skidding under high-speed and low-load conditions [2]. It will generate too much heat, leading to the sliding damage of the bearing and further causing the engine to fail to run properly. To avoid effectively the bearing sliding damage [3], the outer raceway of the bearing is improved from a circular shape to a triple-lobe shape. When the bearing is mounted with interference, the radial clearance [4] relative to the low point circle of the outer triple-lobe raceway becomes negative. Three effective preload areas are formed in the circumferential direction of bearing, and the contact load between the rollers and the inner raceway increases, thereby reducing the risk of skidding.

Ye et al. [5] established a quasi-dynamic model of high speed cylindrical roller bearings, and analyzed the effects of rotational speed, clearance, external load and rollers tilted on the bearing load distribution; Ren et al. [6] proposed a contact load distribution calculation method of bearing under the different clearance conditions, and the results are similar by comparing the proposed method with the Harris method; Oswald et al. [7] researched the effects of radial clearance on the fatigue life and load distribution of bearings, and an improved Stribeck formula was proposed to analyze the effect of radial clearance on the maximum contact load; Lazovic et al. [8] analyzed the effects of the number of rolling elements, internal radial clearance and external load on the load distribution; Nagatomo et al. [9] studied the effects of load distribution on the life of roller bearings; Chen et al. [10] proposed a static analysis model to study the effect of roller diameter difference on bearing load distribution; Tomovic et al. [11] proposed a numerical model that takes into account the two cases of even and odd rollers supporting the inner ring and analyzed the effect of the bearing internal structure on the load distribution; Hao and Demirhan [12,13] established the finite element model of cylindrical roller bearing, calculated the displacement of the bearing ring, and carried out the test verification; Cavallaro et al. [14] established the bearing model with flexible rings to discuss the load distribution, contact pressure and heat dissipation; Oswald and Fujiwara [15,16] analyzed the effect of roller design on bearing performance. However, the raceway of cylindrical roller bearings studied above is circular, and the preload distribution of the bearing is not considered.

Deng et al. [17] established the nonlinear dynamic differential equations of cylindrical roller bearing with triple-lobe raceway and analyzed the influences of the

* e-mail: yuqingjie6147@126.com

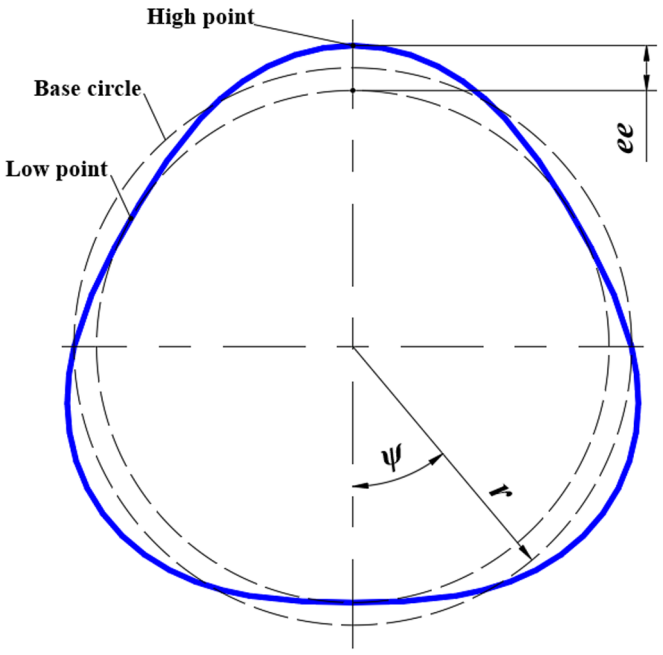

Fig. 1. The schematic diagram of the triple-lobe profile.

different raceway structures, working conditions and outer ring mounted angles on the cage slip ratio. However, when the bearing rotates, the change in the number of loaded rollers and the contact load is not considered, and the preload state of the bearing is not analyzed.

In this paper, considering the radial load and moment conditions, a quasi-static model of cylindrical roller bearing with triple-lobe raceway is established and an improved Newton-Raphson method to solve the numerical model is proposed. For the two states of single-pressed and double-pressed, the contact load distribution of bearing with triple-lobe raceway is analyzed, and the effects of mounting radial clearance, outer triple-lobe raceway waveform value, radial load and rotational speed on inner raceway maximum contact load and preload are investigated. At the same time, the bearing temperature trend predicted by the preload characteristic is verified by the test. It shows the numerical model is effective.

2 Numerical model of cylindrical roller bearing with triple-lobe raceway

2.1 Assumptions

To facilitate the analysis of bearing preload characteristics, the numerical model adopts the following assumptions:

– The outer ring is fixed in space and the inner ring rotates at a constant speed with a fixed axis.
– Each part of the bearing is rigid and only local contact deformation is considered.
– The numerical model ignores the effects of lubrication, friction, heat and cage on the bearing.
– The linear velocity of the contact point of the roller with the inner raceway and the outer raceway is equal to the linear velocity of the raceway at that point.

2.2 Outer raceway triple-lobe curve

The triple-lobe wave curve is periodic in the circumferential direction. To establish the numerical model of cylindrical roller bearing with triple-lobe raceway, the equation of triple-lobe is proposed. The schematic diagram of the triple-lobe profile is shown in Figure 1.

The polar coordinate equation of the triple-lobe curve is:

$$\rho = r - 0.5ee * \cos(3\psi). \tag{1}$$

2.3 Force analysis of bearing with triple-lobe raceway

The cylindrical roller bearing with triple-lobe raceway will generate internal contact loads at the three low point areas of the waveform after mounting. During the bearing operation, the maximum contact load position is always changing between one position (roller is facing the low point of the triple-lobe raceway) and the other position (roller moves half of the roller position angle from the low point of the triple-lobe raceway). The load state that the roller is facing the low point of the triple-lobe raceway is defined as "single-pressed", The load state that the roller moves half of the roller position angle from the low point of the triple-lobe raceway is defined as "double-pressed". The contact loads of single-pressed and double-pressed states are two extreme loads. The contact load of the transition region is between the two extreme contact loads.

The preload distribution of cylindrical roller bearing with triple-lobe raceway before loading in the single-pressed and double-pressed states is shown in Figure 2. When the bearing is subjected to an external load, the internal contact load will change. The preload distribution of cylindrical roller bearing with triple-lobe raceway after loading in the single-pressed and double-pressed states is shown in Figure 3.

In Figure 3, O_1 and O_2 are the center points of the inner ring before loading and after loading, F_r is the radial load, δ_r is the radial displacement of the inner ring after loading, ψ_j is the position angle of the jth roller, ω_i is the inner ring angular speed, G_r is the radial clearance relative to the low point circle of the outer triple-lobe raceway, which can be expressed as

$$G_r = 2r - ee - 2D_w - d_i. \tag{2}$$

Assuming that the number of rollers is Z, the position angle [18] of the jth roller is:

$$\psi_j = \psi_1 + 2\pi(j-1)/Z \tag{3}$$

when the roller rotates with the inner ring, the position angle of the roller will change, and the value of ψ_1 needs to be adjusted in the numerical model.

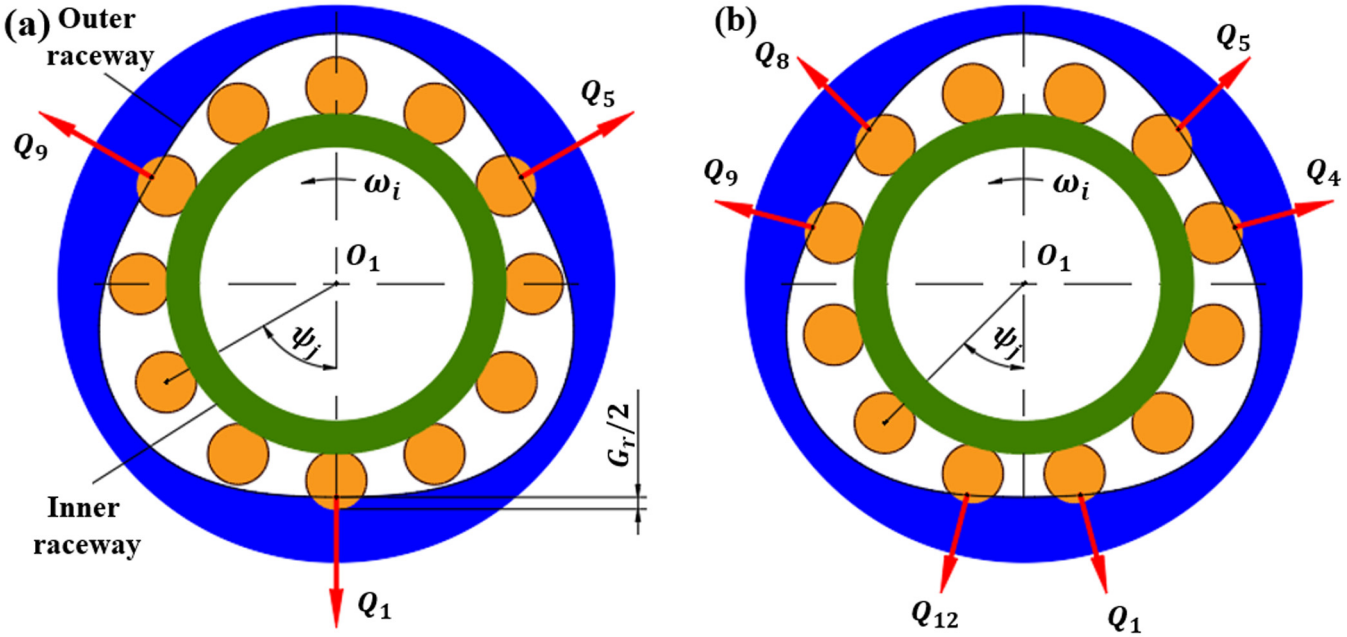

Fig. 2. Preload distribution of the cylindrical roller bearing with triple-lobe raceway before loading: (a) single-pressed state; (b) double-pressed state.

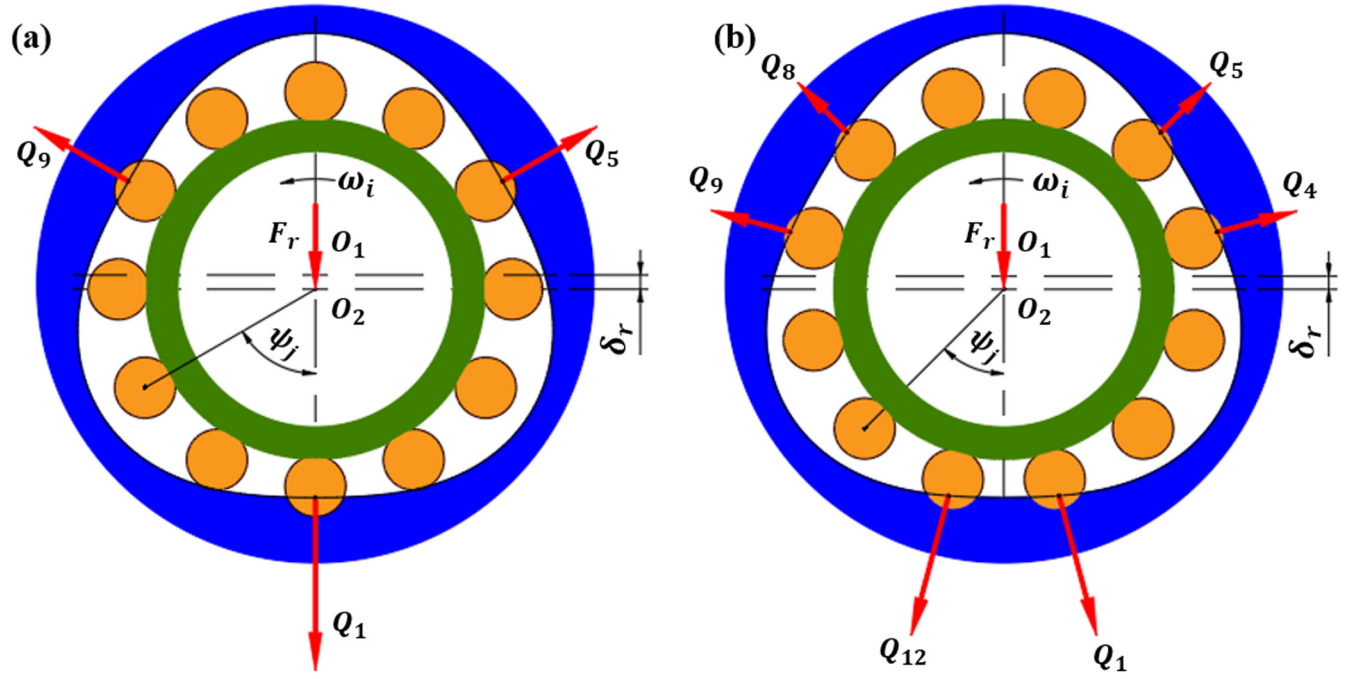

Fig. 3. Preload distribution of the cylindrical roller bearing with triple-lobe raceway after loading: (a) single-pressed state; (b) double-pressed state.

2.3.1 Force analysis of roller

When the bearing is subjected to the radial load F_r, moment M and high-speed centrifugal load, the inner ring will happen a radial displacement δ_r and a misalignment angle θ relative to the outer ring [19], and the contact load at each roller position will vary. Considering the profile modification of rollers, the slicing method [20] is used in the numerical model. The roller effective length is L_{we}, the number of slices is N, and the roller slice thickness is λ. The schematic diagram of the bearing contact model is shown in Figure 4.

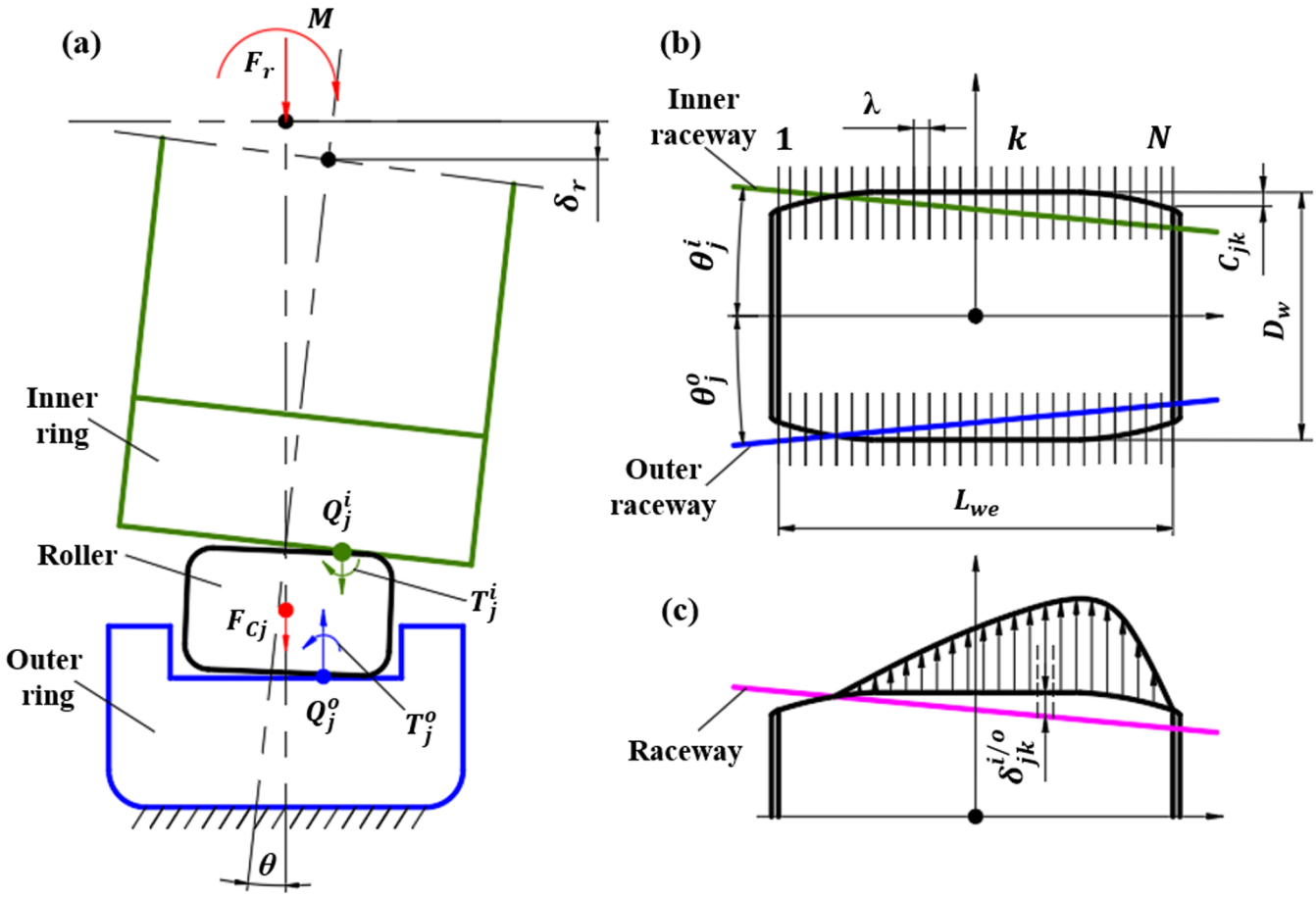

Fig. 4. Schematic diagram of bearing contact model: (a) bearing cross-section geometry and roller force; (b) schematic diagram of slicing method; (c) schematic diagram of contact deformation.

The force balance equations [21] of the jth roller are:

$$\begin{cases} Q_j^i - Q_j^o + F_{Cj} = 0 \\ T_j^i - T_j^o = 0 \end{cases}. \tag{4}$$

The centrifugal force of the jth roller is

$$F_{Cj} = 0.5 m_w d_m w_{mj}^2. \tag{5}$$

The contact load and moment of the jth roller on the inner raceway and outer raceway are:

$$\begin{cases} Q_j^i = \sum_{k=1}^{k=N} q_{jk}^i \\ Q_j^o = \sum_{k=1}^{k=N} q_{jk}^o \\ T_j^i = \sum_{k=1}^{k=k} q_{jk}^i \left(-\frac{L_{we}}{2} + k\lambda \right) \\ T_j^o = \sum_{k=1}^{k=k} q_{jk}^o \left(-\frac{L_{we}}{2} + k\lambda \right). \end{cases} \tag{6}$$

The contact slice loads of the kth slice of the jth roller on the inner raceway and outer raceway are:

$$\left\{ q_{jk}^i = K_k^i \cdot \delta_{jk}^{i} 10/9 \, , \delta_{jk}^i > 0 q_{jk}^o = K_k^o \cdot \delta_{jk}^{o} 10/9, \delta_{jk}^o > 0 \right. \tag{7}$$

The contact elastic deformations of the kth slice of the jth roller on the inner raceway and outer raceway are:

$$\begin{cases} \delta_{jk}^i = \delta_j^i + \left(-\frac{L_{we}}{2} + k\lambda \right) \theta_j^i - C_{jk} \\ \delta_{jk}^o = \delta_j^o + \left(-\frac{L_{we}}{2} + k\lambda \right) \theta_j^o - C_{jk} \end{cases}. \tag{8}$$

The relationship between the contact deformation δ_j^i of the jth roller relative to the inner raceway, the contact deformation δ_j^o of the jth roller relative to the outer raceway and the inner ring radial displacement δ_r is:

$$\delta_j^i = \delta_r \cos(\psi_j) - \frac{G_r}{2} - \delta_j^o - 0.5ee + 0.5ee * \cos(3\psi_j). \tag{9}$$

The relationship between the misalignment angle θ_j^i of the jth roller relative to the inner raceway, the misalignment angle θ_j^o of the jth roller relative to the outer raceway,

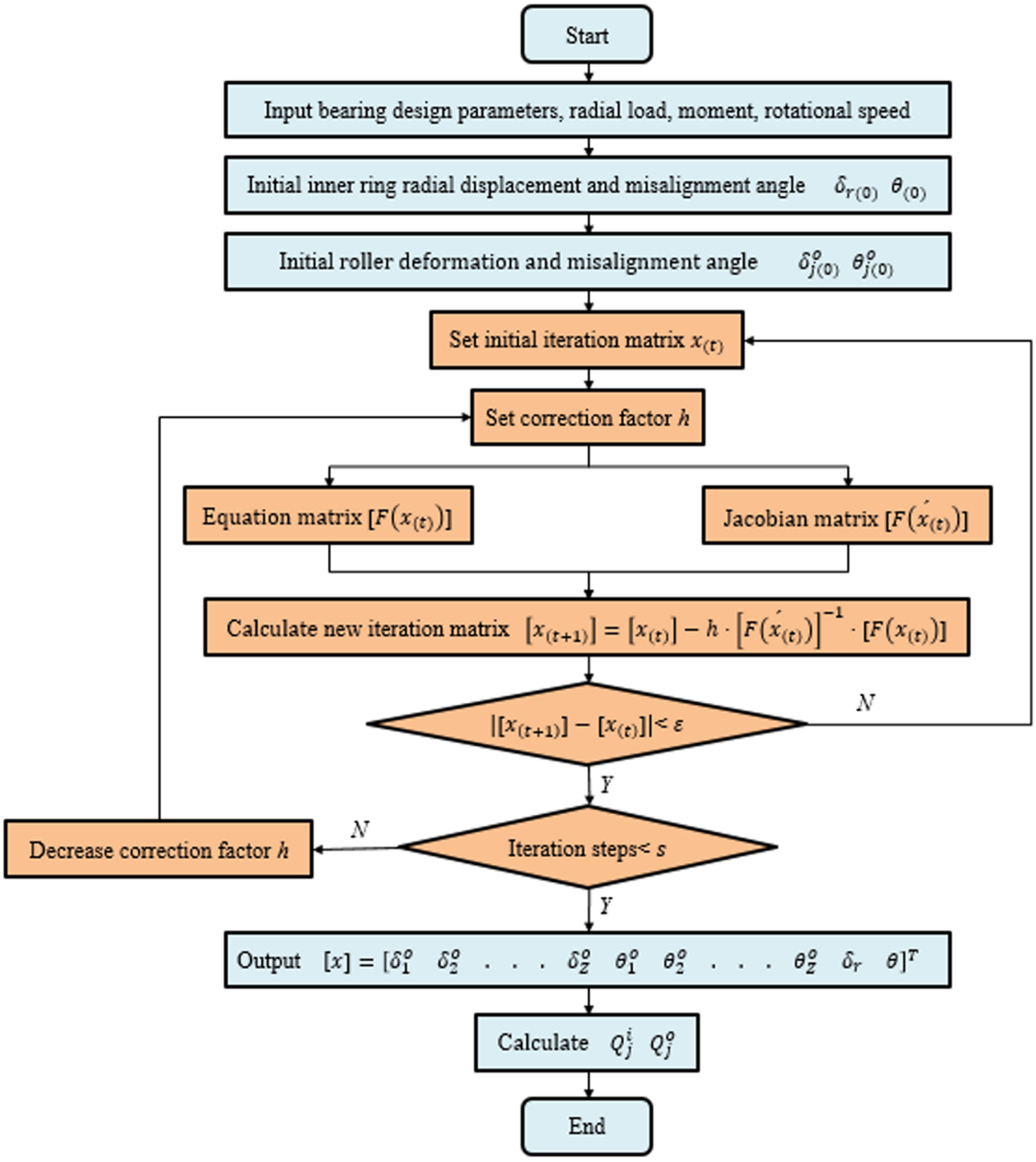

Fig. 5. The solution procedure of numerical model.

and the inner ring misalignment angle θ is:

$$\theta^i_j = \theta\cos(\psi_j) - \theta^o_j. \tag{10}$$

2.3.2 Overall force analysis of bearing

When the bearing is subjected to the radial load F_r and moment M, the external load is shared between each roller and inner raceway. The contact load between the roller and the inner raceway is accumulated to form the overall force balance equations of bearing [22,23], it is expressed as

$$\begin{cases} F_r - \sum_{j=1}^{j=Z} Q^i_j \cos(\psi_j) = 0 \\ M - \sum_{j=1}^{j=Z} T^i_j \cos(\psi_j) = 0 \end{cases}. \tag{11}$$

Table 1. Bearing parameter.

Project	Parameter	Project	Parameter
Inner ring diameter (mm)	50	Inner raceway diameter (mm)	54.5
Outer ring diameter (mm)	73	Number of rollers	18
Initial radial clearance (mm)	0.003	Roller diameter (mm)	7
Mounting radial clearance (mm)	–0.015	Roller length (mm)	7
Outer raceway waveform value (mm)	0.06		

2.4 Solution of the numerical model

Substituting equation (5) through equation (10) into equation (4) and equation (11), it forms an equation matrix [24] with δ_j^o, θ_j^o, δ_r, θ totaling (2Z+2) unknowns, and the matrix is defined as $[F(x_{(t)})]$. The matrix $[F(x_{(t)})]$ is expressed as

$$[F(x_{(t)})] = \begin{bmatrix} Q_1^i - Q_1^0 + F_{C1} \\ Q_2^i - Q_2^0 + F_{C2} \\ \cdot \\ \cdot \\ \cdot \\ Q_Z^i - Q_Z^0 + F_{CZ} \\ T_1^i - T_1^0 \\ T_2^i - T_2^0 \\ \cdot \\ \cdot \\ \cdot \\ T_Z^i - T_Z^0 \\ F_r - \sum_{j=1}^{j=Z} Q_j^i \cos(\psi_j) \\ M - \sum_{j=1}^{j=Z} T_j^i \cos(\psi_j) \end{bmatrix} = \begin{bmatrix} 0 \\ 0 \\ \cdot \\ \cdot \\ \cdot \\ 0 \\ 0 \\ 0 \\ \cdot \\ \cdot \\ \cdot \\ 0 \\ 0 \\ 0 \end{bmatrix}. \quad (12)$$

The unknown matrix $[x_{(t)}]$ is expressed as

$$[x_{(t)}] = [\delta_1^o \quad \delta_2^o \quad . \quad . \quad . \quad \delta_Z^o \quad \theta_1^o \quad \theta_2^o \quad . \quad . \quad . \quad \theta_Z^o \quad \delta_r \quad \theta]^T \quad (13)$$

Taking the derivative of the matrix $[F(x_{(t)})]$ to the unknown matrix, the (2Z+2)×(2Z+2) order Jacobian matrix can be obtained, which is defined as $[F(x'_{(t)})]$.

To obtain good convergence, a variable correction coefficient $h(0 < h < 1)$ is introduced based on the Newton-Raphson method. The improved Newton-Raphson method [25] is expressed as

$$[x_{(t+1)}] = [x_{(t)}] - h \cdot [F(x'_{(t)})]^{-1} \cdot [F(x_{(t)})]. \quad (14)$$

The solution procedure of the numerical model is shown in Figure 5.

1) The improved Newton-Raphson method has a faster calculation speed, but it is still sensitive to the initial value. The initial value setting needs to first solve the initial radial displacement $\delta_{r(0)}$ and initial misalignment angle $\theta_{(0)}$ of the inner ring according to bearing design parameters, radial load, moment and rotational speed.

$$\delta_{r(0)} = \left(\frac{4.08F_r}{ZK_n}\right)^{0.9} + 0.5G_r + 0.5ee - 0.5ee * \cos\left(\min\left(3\psi_1, \frac{6\pi}{Z} - 3\psi_1\right)\right), \psi_1 \le \frac{2\pi}{Z} \quad (15)$$

$$\theta_{(0)} = \frac{G_r + ee - ee * \cos\left(min\left(3\psi_1, \frac{6\pi}{Z} - 3\psi_1\right)\right)}{L_{we}}. \quad (16)$$

If $\theta_{(0)} \le 0$, set $\theta_{(0)} = 1 \times 10^{-10}$.

2) According to the initial radial displacement $\delta_{r(0)}$ and initial misalignment angle $\theta_{(0)}$ of the inner ring, further estimate the contact deformation $\delta_{j(0)}^o$ and misalignment angle $\theta_{j(0)}^o$ of the jth roller relative to the outer raceway.

$$\delta_{j(0)}^o = 0.5\delta_r \cos(\psi_j) - 0.25G_r - 0.25ee + 0.25ee * \cos(3\psi_j). \quad (17)$$

If $\delta_{j(0)}^o \le 0$, set $\delta_{j(0)}^o = 1 \times 10^{-10}$.

$$\theta_{j(0)}^o = 0.5\theta_{(0)} \cos(\psi_j). \quad (18)$$

3) Bring the initial value into the equation matrix $[F(x_{(t)})]$ and Jacobian matrix $[F(x'_{(t)})]$ to calculate the new initial value by equation (14), and start the iterative calculation. It will stop until the calculation error $\Delta x = |x_{(t+1)} - x_{(t)}|$ is less than the allowable error ε, and the number of iteration steps is less than the number of set iteration steps S. When it does not converge after reaching the number of set iteration steps S, the iterative calculation is performed again by reducing the correction coefficient h.

3 Analysis and discussion

Taking a cylindrical roller bearing with triple-lobe raceway as an example, the main parameters of the bearing are shown in Table 1. The initial radial clearance of the bearing is positive. When the bearing is mounted on the shaft with interference, the mounting radial clearance will become negative. It can be calculated by the elastic thickness ring theory [1]. The bearing material is M50, the radial load is 100 N, and the inner ring rotational speed is 40,000 r/min. Due to the different bearing structures, lubrication conditions and load conditions, the temperature distribu-

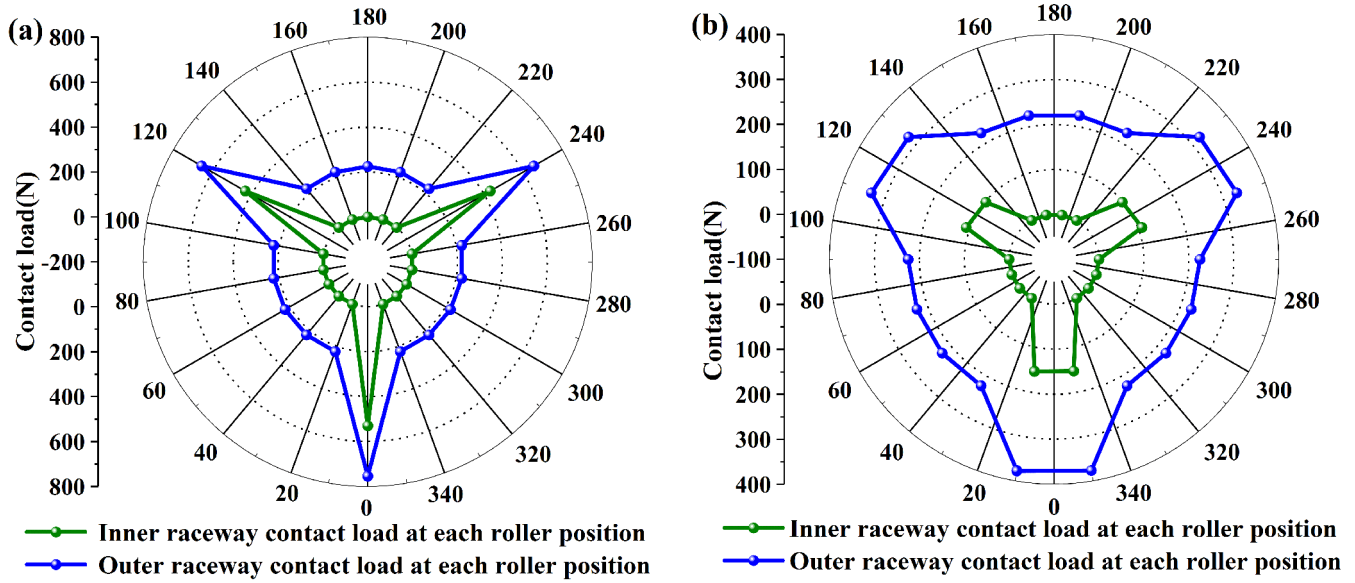

Fig. 6. The contact load distribution: (a) single-pressed state; (b) double-pressed state.

Table 2. Comparison between the improved Newton-Raphson method and the original Newton-Raphson method.

State	Method	Number of iteration steps	Convergent or divergent
Single-pressed	Newton-Raphson	11	Convergent
	Improved Newton-Raphson	8	Convergent
Double-pressed	Newton-Raphson	–	Divergent
	Improved Newton-Raphson	14	Convergent

tion of bearing is always changing, and it is difficult to estimate. So the following analysis model ignores the thermal effect on the bearing, and it only considers the contact load and preload characteristics of the bearing under the mounting radial clearances. The bearing contact load distribution is shown in Figure 6. The cylindrical roller bearing with triple-lobe raceway has three preload areas, and the maximum preload area is along the radial load direction. For the single-pressed state, the number of loaded rollers is 3. For the double-pressed state, the number of loaded rollers is 6. Compared with the single-pressed state, the contact load and preload decrease with the increase in the number of loaded rollers.

The comparison between the improved Newton-Raphson method and the original Newton-Raphson method is shown in Table 2. The improved Newton-Raphson method has better convergence than the original Newton-Raphson method.

Since the effect of lubrication is ignored in the numerical model, the Hamrock and Dowson theory is used to further analyze the lubricating oil film thickness. Under the above conditions, the average temperature monitored by the bearing test is 123.5 °C, so the MIL-PRF-23699 lubricating oil properties at 123.5 °C are used. The results of contact deformation and oil film thickness are shown in Table 3. It can provide a reference for future scholars to supplement the numerical model.

3.1 Effect of mounting radial clearance on maximum contact load and preload of the inner raceway

Under the conditions of radial load 100 N and rotational speed 40,000 r/min, the maximum contact load variation of the inner raceway and the number of loaded rollers variation under the different mounting radial clearances are shown in Figure 7. As the mounting radial clearance increases, the maximum contact load of the inner raceway decreases, and the number of loaded rollers decreases gradually. For the rollers in the single-pressed state, when the number of loaded rollers is reduced to 1, the maximum contact load of the inner raceway remains unchanged, and the bearing preload disappears. For the rollers in the double-pressed state, when the number of loaded rollers is reduced to 2, the maximum contact load of the inner raceway remains unchanged, and the bearing preload disappears. As the mounting radial clearance increases, the preload in the double-pressed state disappears earlier than that in the single-pressed state. The results show that when the mounting radial clearance value of

Table 3. The results of contact deformation and oil film thickness.

Single-pressed state		Double-pressed state	
Project	Parameter (μm)	Project	Parameter (μm)
Inner raceway contact deformation	3.5	Inner raceway contact deformation	1.2
Outer raceway contact deformation	4.7	Outer raceway contact deformation	2.7
Inner raceway oil film thickness	0.22	Inner raceway oil film thickness	0.26
Outer raceway oil film thickness	0.24	Outer raceway oil film thickness	0.27

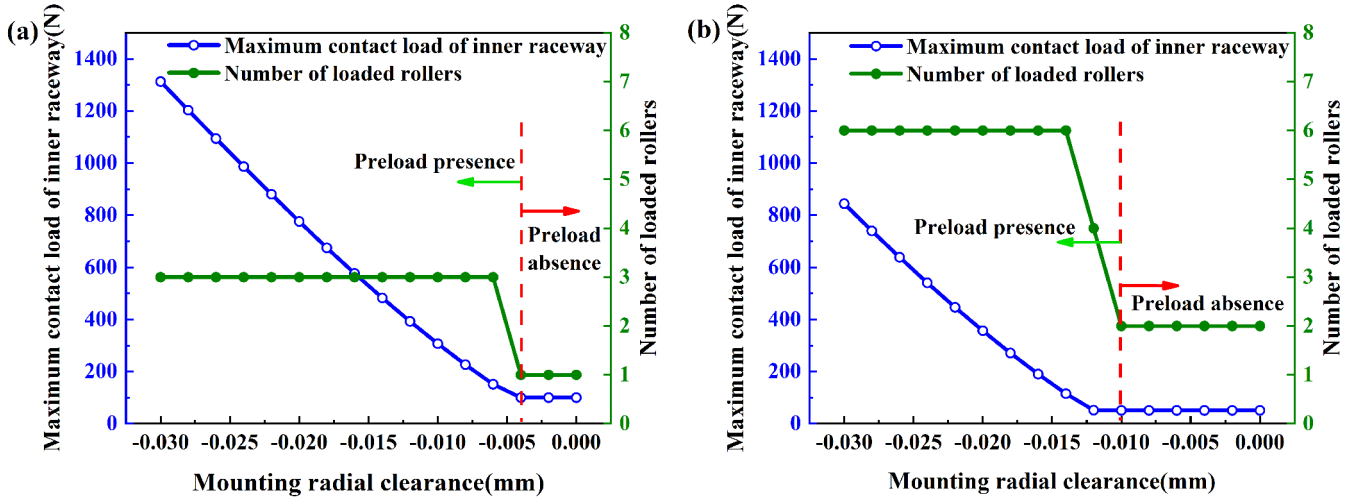

Fig. 7. The maximum contact load variation of the inner raceway and the number of loaded rollers variation under the different mounting radial clearances: (a) single-pressed state; (b) double-pressed state.

cylindrical roller bearing with triple-lobe raceway is designed, it is necessary to first consider the double pressure state to ensure that the bearing preload always exists.

3.2 Effect of outer raceway waveform value on maximum contact load and preload of the inner raceway

Under the conditions of radial load 100 N and rotational speed 40,000 r/min, the maximum contact load variation of the inner raceway and the number of loaded rollers variation under the different outer raceway waveform values are shown in Figure 8. For the single-pressed state, as the outer raceway waveform value increases, the maximum contact load of the inner raceway increases, and the number of loaded rollers decreases. When the number of loaded rollers is reduced to 3, the maximum contact load of the inner raceway remains unchanged, and the bearing preload always exists. For the double-pressed state, as the outer raceway waveform value increases, the maximum contact load of the inner raceway decreases, and the number of loaded rollers decreases. When the number of loaded rollers decreases to 2, the maximum contact load of the inner raceway remains unchanged, and the bearing preload disappears. The smaller the outer raceway waveform value, the greater the number of loaded rollers, and the more loaded rollers will cause the bearing to overheat, which is confirmed in subsequent tests. As the outer raceway waveform value increases, the improvement of overheating in the single-pressed state is later than that in the double-pressure state, and the bearing preload in the double-pressed state disappears earlier than that in the single-pressure state. The results show that the single-pressed state should be considered to prevent the bearing overheating in the design of the lower limit of outer raceway waveform value, and the double-pressed state should be considered to ensure the bearing preload always exists in the design of the upper limit of outer raceway waveform value.

3.3 Effect of radial load on maximum contact load and preload of the inner raceway

Under the condition of rotating speed 40,000 r/min, the maximum contact load variation of the inner raceway and the number of loaded rollers variation under the different radial loads are shown in Figure 9. For the single-pressed state, within a certain load range, as the radial load increases, the maximum contact load of the inner raceway increases, the number of loaded rollers remains unchanged and the bearing preload always exists. For the double-pressed state, as the radial load increases, the radial displacement of the inner ring increases, the maximum

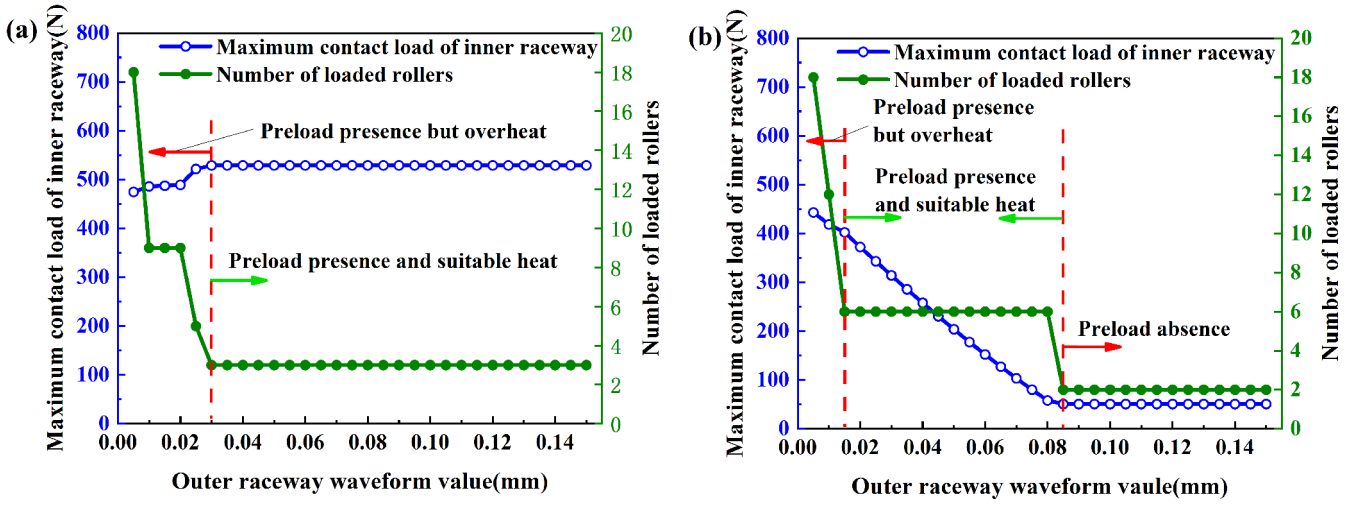

Fig. 8. The maximum contact load variation of the inner raceway and the number of loaded rollers variation under the different outer raceway waveform values: (a) single-pressed state; (b) double-pressed state.

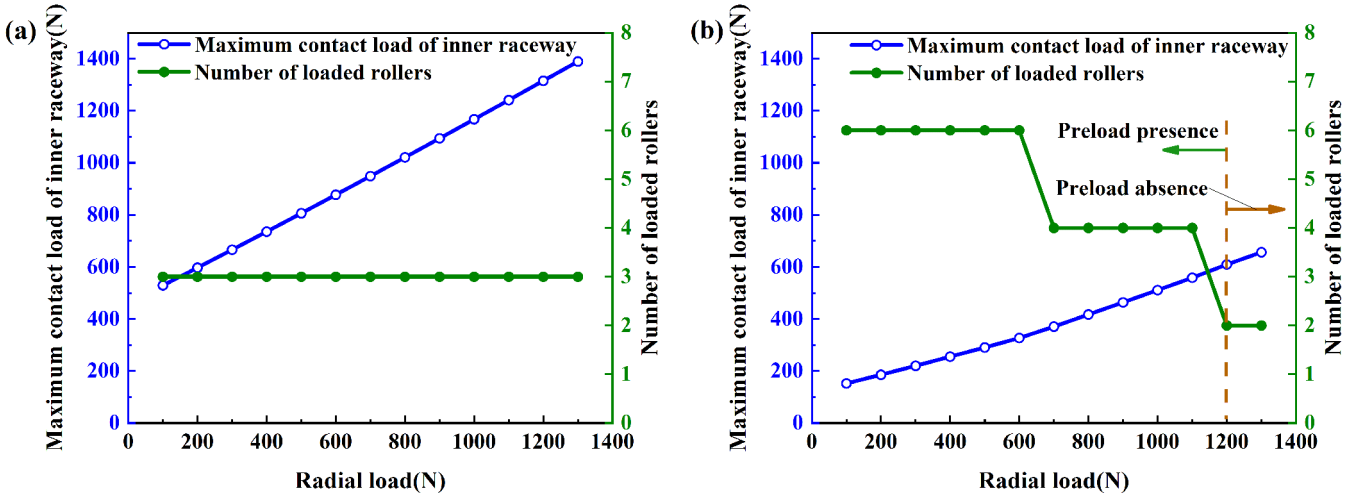

Fig. 9. The maximum contact load variation of the inner raceway and the number of loaded rollers variation under the different radial loads: (a) single-pressed state; (b) double-pressed state.

contact load of the inner raceway increases, and the number of loaded rollers decreases. When the number of loaded rollers is reduced to 2, the bearing preload disappears. The results show that the double-pressed state needs to be considered in designing the outer raceway triple-lobe structure to ensure the bearing preload always exists according to the radial load condition.

3.4 Effect of rotational speed on maximum contact load and preload of the inner raceway

Under the condition of radial load 100N, the maximum contact load variation of the inner raceway and the number of loaded rollers variation under the different inner ring rotational speeds are shown in Figure 10. For the single-pressed state, within a certain speed range, as the inner ring rotational speed increases, the centrifugal load increases, the maximum contact load of the inner raceway decreases, the number of loaded rollers remains unchanged and the bearing preload always exists. For the double-pressed state, as the inner ring rotational speed increases, the maximum contact load of the inner raceway decreases, and the number of loaded rollers decreases. When the number of loaded rollers is reduced to 2, the bearing preload disappears. The results show that the double-pressed state needs to be considered in designing the outer raceway triple-lobe structure to ensure the bearing preload always exists according to the inner ring rotational speed condition.

4 Verification

The cylindrical roller bearing with triple-lobe raceway mainly reduces the internal sliding frictional heat through preload, preventing the bearing from overheating and

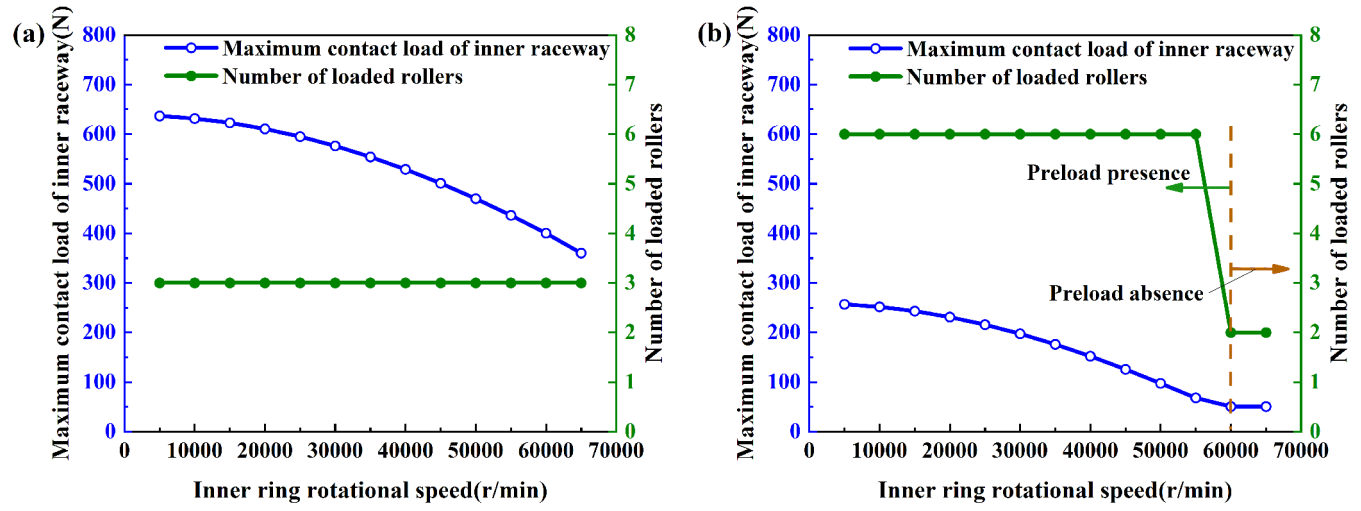

Fig. 10. The maximum contact load variation of inner raceway and the number of loaded rollers variation under the different inner ring rotational speeds: (a) single-pressed state; (b) double-pressed state.

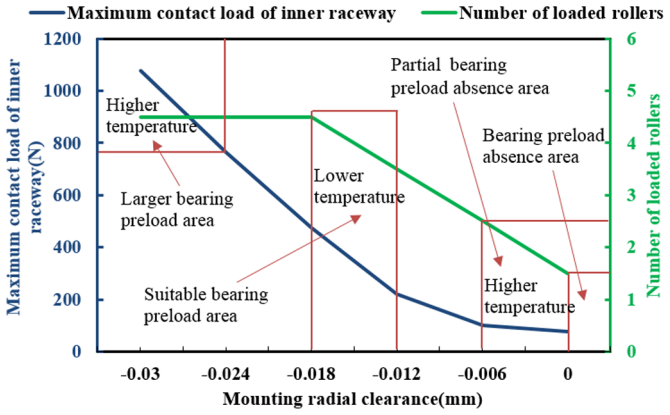

Fig. 11. The preload characteristics and temperature trend prediction of bearing under the different mounting radial clearances.

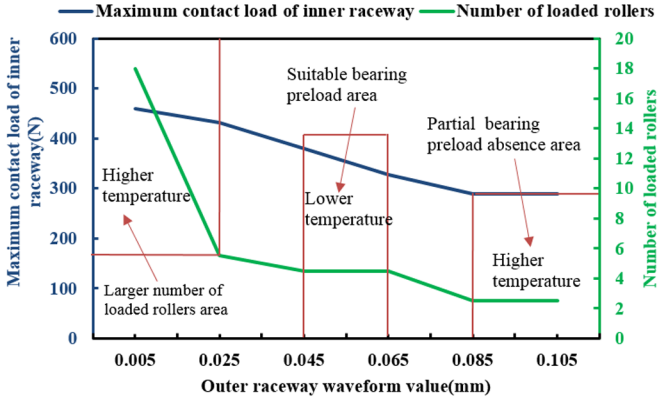

Fig. 12. The preload characteristics and temperature trend prediction of bearing under the different outer raceway waveform values.

damage under high-speed and light-load conditions. When the bearing preload is insufficient or excessive, the bearing temperature will increase. Therefore, the temperature of the cylindrical roller bearing with triple-lobe raceway can also reflect the bearing preload.

We average the two states in Figure 7 to obtain the preload characteristics and predict the temperature trend of bearing under the different mounting radial clearances, which is shown in Figure 11. As the mounting radial clearance increases, the predicted temperature first decreases and then increases.

We average the two states in Figure 8 to obtain the preload characteristics and predict the temperature trend of bearing under the different outer raceway waveform values, which is shown in Figure 12. As the outer raceway waveform value increases, the predicted temperature first decreases and then increases.

To verify the predicted temperature trend, bearing tests with different mounting radial clearances and outer raceway waveform values are carried out to monitor the bearing temperature. The basic parameters of the bearing are shown in Table.1, the variable parameters of the test bearing are shown in Table 4, and the layout of the tester is shown in Figure 13. The test uses two preloaded ball bearings as support bearings. The lubricant type is MIL-PRF-23699, the lubrication method is jet lubricated, the oil flow is 1.5 L/min, and the inlet oil temperature is 75 °C. Bearing temperature is measured to use two similar size cylindrical roller bearings with triple-lobe raceway per test, and the average temperature of bearing in the stable phase is used as the final temperature due to the large amount of bearing temperature data. The load on the two support bearings is 200 N, and the shaft rotational speed is 40,000 r/min. Under the current test conditions, the bearing temperature under the different mounting radial clearances is shown in Figure 14, and the bearing temperature under the different outer raceway waveform values is shown in Figure 15. The test temperature trend is consistent with the predicted temperature trend of the preload characteristics. It shows that the larger preload, the preload absence or the more loaded rollers will generate a lot of heat and cause the temperature to rise.

Table 4. Variable parameters of the test bearing.

Serial number	Mounting radial clearance (mm)	Serial number	Outer raceway waveform value (mm)
1	–0.03	7	0.005
2	–0.024	8	0.025
3	–0.018	9	0.045
4	–0.012	10	0.065
5	–0.006	11	0.085
6	0	12	0.105

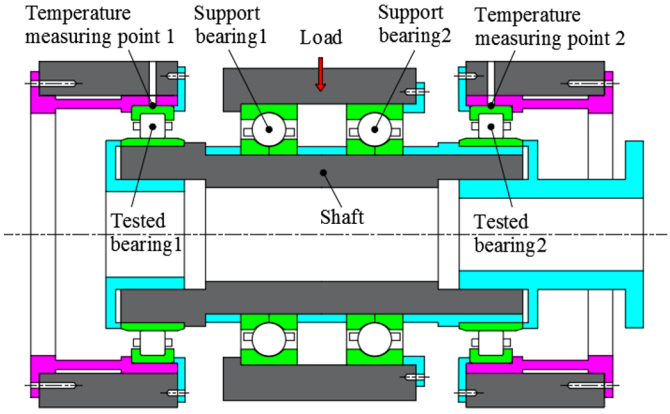

Fig. 13. Layout of the tester.

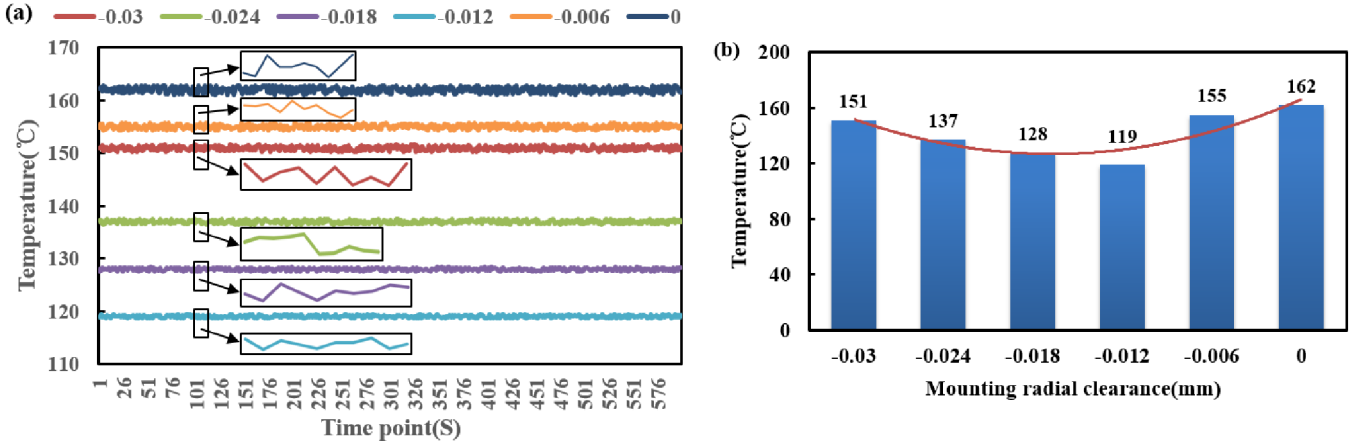

Fig. 14. Bearing temperature under the different mounting radial clearances: (a) Time point temperature in the stable phase; (b) average temperature.

5 Conclusions

In the paper, the quasi-static numerical analysis model of cylindrical roller bearing with triple-lobe raceway is established and solved by the improved Newton-Raphson method. The effects of mounting radial clearance, outer raceway waveform value, radial load and rotational speed on the maximum contact load and preload of cylindrical roller bearing with triple-lobe raceway are investigated. The temperature trend of the test is consistent with the predicted temperature trend of preload characteristics. It shows that the larger preload, the preload absence or the more loaded rollers will generate a lot of heat and cause the temperature to rise.

– A quasi-static analysis model of cylindrical roller bearing with triple-lobe raceway is established, and an improved Newton-Raphson method to solve the model is proposed.
– According to the radial load and rotational speed conditions of the bearing, the double-pressed state needs to be considered in designing the outer raceway triple-lobe structure to ensure the bearing preload always exists.

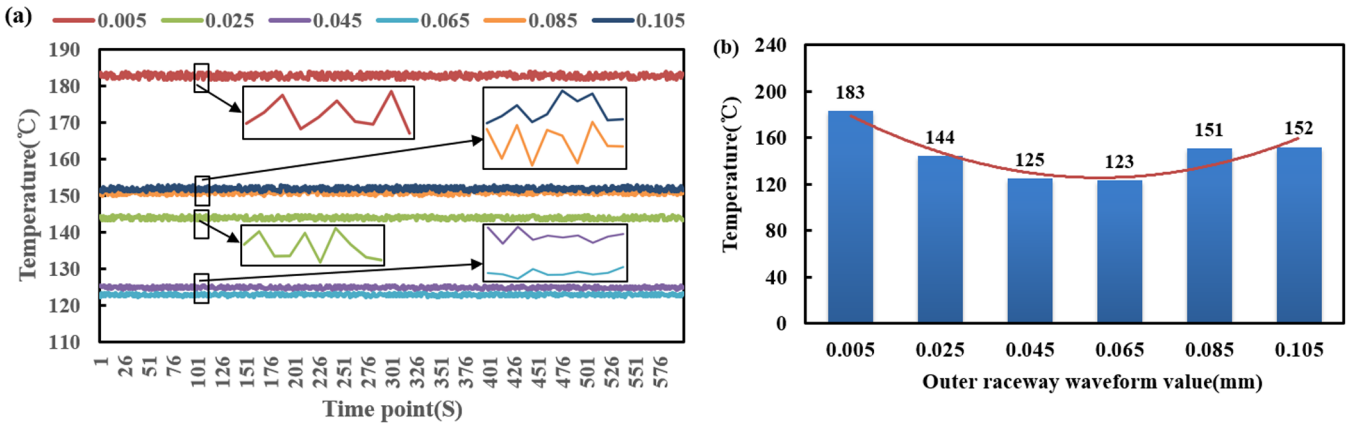

Fig. 15. Bearing temperature under the different outer raceway waveform values: (a) Time point temperature in the stable phase; (b) average temperature.

– In the design of the mounting radial clearance value of cylindrical roller bearing with triple-lobe raceway, it is necessary to consider first the double-pressed state to ensure the bearing preload always exists.
– In the design of the lower limit of the outer raceway waveform value, it is necessary to consider the single-pressed state to prevent the bearing overheating, and in the design of the upper limit of the outer raceway waveform value, it is necessary to consider the double-pressed state to ensure the bearing preload always exists.

Nomenclature

r	Radius of triple-lobe curve base circle
ee	Triple-lobe curve waveform value
G_r	Bearing radial clearance
D_w	Roller diameter
d_i	Inner raceway diameter
m_w	Mass of the roller
d_m	Diameter of the pitch circle
L_{we}	Roller effective length
λ	Thickness of roller slice
C	Roller convexity drop amount
F_r	Bearing radial load
M	Moment
δ_r	Radial displacement of inner ring
θ	Misalignment angle of inner ring
ψ	Roller position angle
ω_i	Inner ring angular speed
ω_{mj}	Revolution angular speed of the roller j
Q	Contact load
T	Contact moment
q	Slice load
F_{Cj}	Centrifugal force of roller j
K_n	Bearing contact stiffness
Z	Number of rollers
N	Number of slices
δ_j^i	Deformations at the roller/inner raceway contact
δ_j^o	Deformations at the roller/outer raceway contact
θ_j^i	Misalignment angle at the roller/inner raceway
θ_j^o	Misalignment angle at the roller/outer raceway
K	Contact stiffness
$x_{(t)}$	Unknown matrix
$[F(x_{(t)})]$	Matrix of equations
$[F(.x_{\cdot t})]$	Derivation of equations matrix
h	Variable correction coefficient

Subscripts

i	Inner raceway
o	Outer raceway
j	Rolling element index
k	Slice index
t	Iteration index

Matrix notations

$[]$	Matrix
$[]^T$	Transposed matrix
$[]^{-1}$	Inversed matrix

The authors gratefully acknowledge the financial support by an independent special fund from the China Aviation Engine Corporation (ZZCX-2018-048) in Beijing, China.

References

[1] T.A. Harris, M.N. Kotzalas, Rolling Bearing Analysis: Advanced Concepts of Bearing Technology, fifth ed. (Taylor & Francis, Florida, 2007)
[2] X. Xie, J. Xu, J. Luo, Analysis of skid damage to cylindrical roller bearing of mainshaft of aeroengine, J. Mech. Sci. Technol. **34**, 3239–3247 (2020)
[3] S.J. Kim, Analytical consideration of the radial clearance to reduce cage slip of the turbo engine roller bearing, J. Mech. Sci. Technol. **35**, 2827–2839 (2021)
[4] A. Chudzik, B. Warda, Effect of radial internal clearance on the fatigue life of the radial cylindrical roller bearing, Ekspolatacja i Niezawodnosc Maintenance Reliab. **21**, 211–219 (2019)

[5] Z.H. Ye, L.Q. Wang, Effect of tilted misalignment on loading characteristics of cylindrical roller bearings, Mech. Mach. Theory **69**, 142–155 (2013)
[6] X.L. Ren, J. Zhai, Calculation of radial load distribution on ball and roller bearings with positive, negative and zero clearance, Int. J. Mech. Sci. **131-132**, 1–7 (2017)
[7] F.B. Oswald, E.V. Zaretsky, Effect of internal clearance on load distribution and life of radially loaded ball and roller bearings, Tribol. Trans. **55**, 245–265 (2012)
[8] T. Lazovic, M. Ristivojevic, Mathematical model of load distribution in rolling bearing, FME Trans. **36**, 189–196 (2008)
[9] T. Nagatomo, K. Takahashi, Effects of load distribution on life of radial roller bearings, J. Tribol. **134**, 1–7 (2012)
[10] G. Chen, F. Mao, Effects of off-sized cylindrical rollers on the static load distribution in a cylinder roller bearing, Proc. Inst. Mech. Eng. J **226**, 687–696 (2012)
[11] R. Tomovic, Investigation of the effect of rolling bearing construction on internal load distribution and the number of active rolling elements, Adv. Mater. Res. **633**, 103–116 (2013)
[12] X. Hao, X.X. Gu, Distribution characteristics of stress and displacement of rings of cylindrical roller bearing, J. Mech. Eng. Sci. **233**, 4348–4358 (2018)
[13] N. Demirhan, B. Kanber, Stress and displacement distributions on cylindrical roller bearing rings using FEM, Mech. Based Des. Struct. Mach. **36**, 86–102 (2008)
[14] G. Cavallaro, D. Nelias, Analysis of high-speed intershaft cylindrical roller bearing with flexible rings, Tribol. Trans. **48**, 153–167 (2005)
[15] F.B. Oswald, E.V. Zaretsky, Effect of roller geometry on roller bearing load-life relation, Tribol. Trans. **57**, 928–938 (2014)
[16] H. Fujiwara, T. Kobayashi, Optimized logarithmic roller crowning design of cylindrical roller bearings and its experimental demonstration, Tribol. Trans. **53**, 909–916 (2010)
[17] S.E. Deng, Y.J. Lu, Cage slip characteristics of a cylindrical roller bearing with a trilobe-raceway, Chin. J. Aeronaut. **879**, 1–12 (2017)
[18] S. Kabus, M.R. Hansen, A new quasi-static multi-degree of freedom tapered roller bearing model to accurately consider non-Hertzian contact pressures in time-domain simulations, Proc. Inst. Mech. Eng. K **228**, 111–125 (2014)
[19] V.C. Tong, S.W. Hong, Characteristics of tapered roller bearing subjected to combined radial and moment loads, Int. J. Precis. Eng. Manufactur. Green Technol. **1**, 323–328 (2014)
[20] S. Deng, J. Gu, Y. Cui, W. Zhang, Dynamic analysis of a tapered roller bearing, Ind. Lubric. Tribol. **70**, 191–200 (2018)
[21] J.M. de Mul, J.M. Vree, Equilibrium and associated load distribution in ball and roller bearings loaded in five degrees of freedom while neglecting friction, J. Tribol. **111**, 153–167 (1989)
[22] S.W. Kwon, V.C. Tong, S.W. Hong, Five-degrees-of-freedom model for static analysis of linear roller bearing subjected to external loading, Proc. Inst. Mech. Eng. C **233**, 2920–2938 (2018)
[23] X. Shi, L. Wang, TEHL analysis of high-speed and heavy-load roller bearing with quasi-dynamic characteristics, Chin. J. Aeronaut. **28**, 1296–1304 (2015)
[24] H. Zhang, W. Shi, G. Liu, Z. Chen, A method to solve the stiffness of double-row tapered roller bearing, Math. Probl. Eng. 1–13 (2019)
[25] T. Nakata, N. Takahashi, K. Fujiwara, N. Okamoto, K. Muramatsu, Improvements of convergence characteristics of Newton-Raphson method for nonlinear magnetic field analysis, IEEE Trans. Magn. **28**, 1048–1051 (1992)

Cite this article as: Q.J. Yu, J. Chi, P. Gong, H.W. Jiang, L.W. Zhan, L.L. Xue, Study on contact load and preload characteristics of cylindrical roller bearings with triple-lobe raceway, Mechanics & Industry **23**, 19 (2022)